New Journal of Physics
The open access journal at the forefront of physics

Deutsche Physikalische Gesellschaft DPG IOP Institute of Physics

PAPER • OPEN ACCESS

XUV fluorescence as a probe of laser-induced helium nanoplasma dynamics

To cite this article: Malte Sumfleth *et al* 2023 *New J. Phys.* **25** 103042

View the article online for updates and enhancements.

You may also like

- Suppression of thermal nanoplasma emission in clusters strongly ionized by hard x-rays
Yoshiaki Kumagai, Zoltan Jurek, Weiqing Xu et al.
- Ionization dynamics of XUV excited clusters: the role of inelastic electron collisions
M Müller, L Schroedter, T Oelze et al.
- Single-shot electron imaging of dopant-induced nanoplasmas
C Medina, D Schomas, N Rendler et al.

This content was downloaded from IP address 131.169.221.241 on 20/10/2023 at 15:36

IOP Publishing New J. Phys. 25 (2023) 103042 https://doi.org/10.1088/1367-2630/ad02b7

New Journal of Physics
The open access journal at the forefront of physics

Deutsche Physikalische Gesellschaft DPG
IOP Institute of Physics

Published in partnership with: Deutsche Physikalische Gesellschaft and the Institute of Physics

OPEN ACCESS

RECEIVED
22 May 2023

REVISED
4 October 2023

ACCEPTED FOR PUBLICATION
12 October 2023

PUBLISHED
20 October 2023

Original Content from this work may be used under the terms of the Creative Commons Attribution 4.0 licence.

Any further distribution of this work must maintain attribution to the author(s) and the title of the work, journal citation and DOI.

PAPER

XUV fluorescence as a probe of laser-induced helium nanoplasma dynamics

Malte Sumfleth[1], **Andreas Przystawik**[1], **Mahesh Namboodiri**[1] **and Tim Laarmann**[1,2,*]

[1] Deutsches Elektronen-Synchrotron DESY, Notkestr. 85, 22607 Hamburg, Germany
[2] The Hamburg Centre for Ultrafast Imaging CUI, Luruper Chaussee 149, 22761 Hamburg, Germany
* Author to whom any correspondence should be addressed.

E-mail: tim.laarmann@desy.de

Keywords: strong-field physics, nanoplasma dynamics, Rydberg state population

Abstract

XUV fluorescence spectroscopy provides information on energy absorption and dissipation processes taking place in the interaction of helium clusters with intense femtosecond laser pulses. The present experimental results complement the physical picture derived from previous electron and ion spectroscopic studies of the generated helium nanoplasma. Here, the broadband XUV fluorescence emission from high-lying Rydberg states that covers the spectral region from $6p \rightarrow 1s$ at 53.0 eV all the way to photon energies corresponding to the ionization potential of He^+ ions at 54.4 eV is observed directly. The cluster size-dependent population of these states in the expanding nanoplasma follows the well-known bottleneck model. The results support previous findings and highlight the important role of Rydberg states in the energetics and dynamics of laser-generated nanoplasma.

1. Introduction

The interaction of strong laser fields with nanoparticles generating plasma at the nanoscale have enjoyed tremendous attention from researchers throughout the last couple of decades [1–4]. Numerous studies have investigated energy deposition and redistribution in atomic and molecular clusters as a function of cluster size situating them between atoms and bulk matter with dimensions down to a few nanometers. Using cluster beams as target material combines the advantage of solid state density of the individual particles with the low target density in the interaction volume. This experimental scheme creates well-defined conditions for studying nanoplasma formation and its relaxation across a large range of excitation energies from the infrared (IR) with laser wavelengths $\lambda > 1\,\mu$m [5], across the VUV [6–11] and XUV spectral range [12, 13] toward x-rays at $\lambda < 10$ nm [14, 15].

Massive electron excitation and ionization generates a deep mean-field potential on the order of keV energy confining the plasma electrons. Enormous electron temperatures beyond 10^6 K can be reached by different mechanisms of energy absorption by the quasifree plasma electrons, which mainly depend on the laser parameters and the particle size. Efficient energy deposition results in the ejection of hot electrons [16], highly charged [17] and energetic ions [18], as well as x-ray emission from the nanoplasma [19]. Even nuclear fusion in laser-heated deuterium clusters has been observed [20].

The optimization of secondary electron, ion, x-ray or pulsed neutron sources toward applications requires detailed knowledge on the evolution of the electronic properties of the expanding nanoplasma driven by the Coulomb forces of ions and the hydrodynamic pressure of electrons. Experimental studies flanked by theoretical calculations show that the electron thermalization to the bottom of the plasma potential is fast. It takes place on a femtosecond (fs) timescale due to the bulk-density conditions and is accompanied by isotropic emission of low-energy (thermal) electrons [21]. During the nanoplasma expansion the binding energy of the quasifree electrons gradually shifts upward forming a delocalized energy band close to the ionization continuum. In this phase, electron-correlation-driven energy transfer processes have to be considered [22–24]. In parallel, the mean-field potential upshift and the resulting increase in the

© 2023 The Author(s). Published by IOP Publishing Ltd on behalf of the Institute of Physics and Deutsche Physikalische Gesellschaft

interatomic Coulomb barriers causes localized states of individual ions to recover [25]. Thereby, triggered by electron–ion recombination processes various additional electronic excitation and energy relaxation channels open up on the picosecond (ps) to nanosecond (ns) time scale [26, 27] including radiative decay [28–30]. This is where the present fluorescence spectroscopy study comes into play to shed light on the less-explored energy redistribution processes in the long-time evolution of a laser-generated helium nanoplasma [31, 32].

Different types of recombination pathways are discussed in the literature [33]. In the radiative recombination of an electron with an ion its excess energy is released as a photon. Three-body recombination (TBR) processes involve two electrons and one ion. One of the two electrons recombines with the ion, while the other electron takes away the excess energy of the first electron. Dielectric recombination describes a variant, where the excess energy is taken up by a second electron already present in the ion, which gets lifted into an electronically excited state. Subsequently, the excited electron relaxes back into its ground state via radiative- or Auger-decay. We note in passing that there exist more complicated recombination processes, such as radiative dielectric recombination, where the radiative decay of the excited electrons happens simultaneously with the initial recombination. In the present work, the focus is on radiative recombination and TBR, because the target is the recombination of quasifree electrons with He^{2+} in a fully ionized He nanoplasma forming He^{+}. Therefore, no other electrons exist in the ion that could participate in dielectric recombination or more complicated processes.

Investigations of the TBR process started back in the 1960s [34] and resulted in the formulation of the so-called classical bottleneck model. The defining features of this model are: (a) the temperature dependence for the total recombination rate, which scales as $\propto T^{-9/2}$, and (b) the electronic state n' most likely being populated is the one with $E_{n'} \sim k_B T$, because its ionization energy is comparable to the kinetic energy of the thermal quasifree electrons. However, for a cold plasma $T < 1000$ K the bottleneck model no longer applies. It neglects quantum effects, such as the increased de Broglie wavelengths of thermal electrons at the bottom of the plasma potential, which enhances the recombination probability and allows for population of states with ionization energies significantly higher than the bottleneck prediction. Furthermore, high l-states of the same n are populated much more frequently in low-temperature plasma compared to the bottleneck regime, where mainly low l-states get populated as outlined in [35]. In the present contribution we apply orbital-sensitive XUV fluorescence spectroscopy relying on dipole selection rules to gain information on laser-generated He nanoplasma dynamics. Our results underline the importance of TBR processes in the energy dissipation during the plasma expansion in agreement with previous works based on electron and ion spectroscopy [31, 32]. Important for these seminal papers on the temporal development of a laser-induced helium nanoplasma, as well as for the present study, is the fact that helium atoms represent one of the simplest atomic systems. In particular, in hydrogen-like He^{+}, the electronic states are energetically degenerate by the orbital momentum quantum number l and electronic transitions result in only a very few fluorescence lines at well-distinguishable photon energies. Fluorescence spectroscopy has been employed before to study laser-induced nanoplasma in heavy rare gas clusters and cluster mixtures comprising more than one element [28–30]. Due to the high number of electrons for heavy rare gases clusters, such as Xe_N, typically a broad charge state distribution is produced in strong laser fields. However, with respect to correlated many-body electronic decay (CED) processes, such as TBR, the characteristic fluorescence from electronically excited states overlap and cannot be experimentally resolved. Hence, the advantage of studying systems like Xe_N to monitor dependencies of extreme charging on the laser pulse properties becomes a disadvantage when studying CED, making experiments on the lighter element helium extremely appealing. Here, the complementary fluorescence data provide evidence that the population of electronically excited states in the transient He nanoplasma follows the bottleneck model.

2. Experimental setup

An overview of the experimental geometry including the key components is given in figure 1. We generate helium clusters by expanding precooled He gas with a purity of 99.9999% from 20 bar stagnation pressure through a circular nozzle into vacuum at temperatures between 4 K and 15 K. The nozzle is formed by an electron microscope aperture plate with a 5 μm orifice, while cooling is provided by a Gifford–McMahon closed-cycle cryostat. This type of He cluster source is well characterized in terms of the temperature and pressure dependent cluster size distribution [36]. By changing the nozzle temperature the average particle size can be tuned from rather small He clusters $\overline{N} = 3.3 \cdot 10^3$ with a diameter on the order of a few nm up to large μm-size droplets comprising more than 10^{10} He atoms. The precision of the temperature control is ± 30 mK, which translates into a size variation, which is much smaller than the full-width at half-maximum of the generated cluster size distribution in a supersonic expansion. The latter is on the order of the average cluster size $\overline{N}$. A few millimeter downstream of the nozzle intense fs laser pulses overlap perpendicularly with the molecular beam.

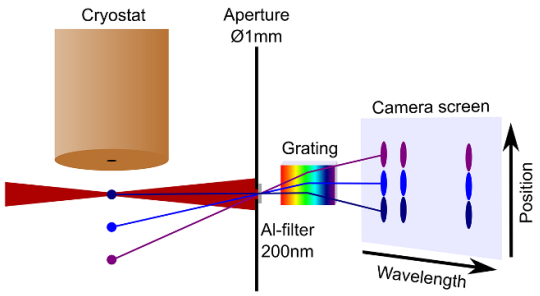

Figure 1. The near-infrared laser beam (red) is focused onto the helium droplets generating a nanoplasma. The emitted XUV fluorescence light is imaged vertically through a pinhole and dispersed horizontally by a grating on a XUV camera chip. Fluorescence emitted from different positions along the droplet beam axis is projected to different locations on the detector and provides information on the population dynamics of electronically excited states, their radiative lifetime and the kinetics of the nanoplasma expansion. The combination of an aluminum filter and the pinhole ensures that the optical laser and stray light is efficiently blocked.

A commercial laser system provides the near-IR pulses with a central wavelength of 1030 nm and a pulse energy of 1 mJ at a repetition rate of 5 kHz. The pulse duration of $\tau = 180$ fs has been characterized by measuring the intensity autocorrelation. The fs pulses are focused onto the He clusters by an $f = 30$ mm lens resulting in a peak intensity beyond 10^{16} W cm^{-2}. Note, the intensity threshold for barrier suppression ionization (BSI) of individual He atoms is $\approx 10^{15}$ W cm^{-2}, while BSI in clusters requires a slightly lower laser intensity [37, 38]. Thus, rather small clusters with an average size $\overline{N} < 10^4$ are almost completely inner-ionized, i.e. the electrons are ionized to a large extent from the individual cluster atoms but do not leave the cluster as a whole, because of the deep plasma potential building up.

Any radiation emitted from the illuminated cluster target in the focal volume has to pass an 1 mm diameter pinhole at a distance of 284 mm from the focus and through a 200 nm-thick aluminum foil, which prevents IR or visible light from entering the spectrometer chamber in the direction of the laser beam propagation further downstream. In addition uncorrelated stray light scattered from metal surfaces in the source chamber is efficiently blocked at the pinhole. The remaining XUV radiation is dispersed by a toroidal variable line-space grating in the spectrometer chamber onto an XUV camera.

At first glance, the spectrometer configuration allows us to detect XUV fluorescence photons emitted in the direction perpendicular to the He cluster jet and parallel to the laser beam propagation. However, it is important to note that the setup with the 1 mm aperture forms a simple pinhole camera as displayed in figure 1. This capability allows to obtain some spatial resolution in the direction of the cluster jet propagation. The location of the detected radiation on the XUV camera chip perpendicular to the dispersion direction of the grating is directly linked to the point in space, where the radiation was emitted. This source point of fluorescence from the expanding He nanoplasma depends on different characteristic velocities and involved time scales, respectively. Clearly, the initial cluster jet speed is small compared to Coulomb explosion and hydrodynamic expansion velocities of the nanoplasma and can be neglected [36]. Thus, the location of emitting ions imaged by the pinhole camera mainly depends on the cluster disintegration, the population dynamics of electronically excited states via TBR and their radiative lifetime.

3. Results and discussion

As the starting point of the present study, we compare the radiative decay of ionized atoms and clusters in figure 2. The experimental procedure is straightforward. It utilizes the fact that the cluster jet is surrounded by a sheath of He atoms that did not condense into clusters. By moving the cryostat so that the laser focus locates spatially either on the sheath of atoms (a) or on the cluster jet (b), one can easily identify the cluster contribution to the recorded XUV fluorescence signal. We like to add that both, the nanoplasma as well as the atomic target emit fluorescence in the visible and IR spectral range. The long-wavelength emission in the direction of the laser beam propagation is blocked by the Al-filter in front of the XUV spectrometer in the present study in order to reduce the signal background. However, we like to note that laser-induced breakdown spectroscopy of helium gas was performed in the past to evaluate its spectral emission characteristics as well as the parameters of the formed plasma, namely electron temperature and electron density (see e.g. [39]).

The radiative decay of irradiated atoms in the XUV spectral range leads to dominant fluorescence lines $3p \rightarrow 1s$ at 25.6 nm, $4p \rightarrow 1s$ at 24.3 nm, $5p \rightarrow 1s$ at 23.7 nm, as well as $6p \rightarrow 1s$ at 23.4 nm of He^+ ions [40]. The vertical length of the fluorescence line in figure 2(a) is given by the 1 mm spatial resolution of the

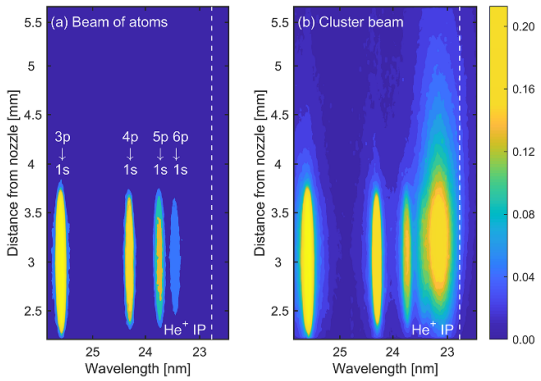

Figure 2. Comparison of the recorded XUV-fluorescence spectra using the pinhole camera, when illuminating (a) atomic helium and (b) clusters comprising on average 1.2×10^6 atoms, which is equivalent to an average particle diameter of about 40 nm. The positions of vertical arrows mark the atomic transition energies [40]. The spectra are normalized to the maximum intensity. The given color scale applies to both spectra.

pinhole camera (limited by the aperture diameter) and folded with the atomic beam velocity and the corresponding fluorescence lifetime. The beam waist at the laser focus perpendicular to the dispersion direction of the XUV grating is much smaller (6 μm). It limits the spectral resolution of the XUV spectrometer and is experimentally determined by the so-called knife-edge method.

In the case of fluorescence emitted from large He clusters the same transitions show up but with an overall higher signal strength and a slightly broadened line spectrum. In addition, also a new dominant contribution appears with a wide wavelength distribution that covers the spectral region from the $6p \rightarrow 1s$ fluorescence all the way to photon energies corresponding to the ionization potential of He^+ ions (22.78 nm and 54.4 eV, respectively) as depicted in figure 2(b). The additional broadband emission has a different vertical profile compared to the fluorescence lines emitted from a beam of atomic He (figure 2(a)). On the first view, one can see that it originates from fluorescing ions emitting further downstream from the nozzle than the initial 3 mm that separate the focus of the drive laser and the nozzle. The center of mass of the broadband emission, i.e. its source point is shifted to a larger distance of 3.3 mm from the nozzle.

The origin of the new broadband emission is radiative transition of $n > 6$ Rydberg states to the 1s state following the population via TBR. Initially, the clusters are field-ionized by the intense laser pulse. During the outer ionization a positive cluster ion core is created, that prevents further outer ionization, while inner ionization continues. This leads to the trapping of quasifree electrons in illuminated He clusters. The created quasifree electrons are driven by the laser field releasing an avalanche of secondary electrons mainly by electron-impact ionization of the surrounding neutral atoms and single charged ions [41]. Note, the presence of ions in the vicinity of He atoms facilitates this ionization cascade, because it lowers their ionization threshold by 10–17 eV [42]. Furthermore, stable He complexes around the ions are formed due to higher binding energy of an ion to the surrounding neutral He atoms compared to the interactions between neutral He atoms [43–45]. These often called 'Atkins snowballs' will be highly mobile in the superfluid and quickly redistribute to minimize the total repulsion energy [46, 47].

In contrast to the positively charged ions building He_n^+ and He_n^{2+} snowballs, whose density can exceed that of solid He, the laser-heated quasifree electrons are heliophobic and form extended void bubbles inside the droplets [48–50]. During the nanoplasma expansion driven by Coulomb and hydrodynamic forces the quasifree electrons cool down sufficiently for TBR to set in. According to the bottleneck model this occurs at an electron temperature where recombination happens predominantly into a small number of n'-quantum number states above $n = 6$ with an ionization energy comparable to the kinetic energy of thermal quasifree electrons. These high-lying Rydberg states then radiatively decay into the 1s-state. The photons from this decay show up on the camera spectrally above the 6p-fluorescence line, which is only weakly populated upon interaction of intense IR pulses with the beam of He atoms.

Also long-lived neutral $He^\star$ excitations in droplets [51–54], which are populated by the recombination of electrons with singly-charged He^+ cations, have been observed in the present experiments. Note, highly excited Rydberg states [55, 56], autoionization [57, 58] and interatomic Coulombic decay processes [59, 60], as well as electronic relaxation leading to the evaporation of Rydberg atoms and excimers (excited dimers) from the droplet surface [58, 61–63] have been studied previously. However, due to the limited performance of the installed XUV grating in the limit of long wavelengths and the presence of spectrally overlapping signals originating from the 2nd diffraction order, we did not evaluate the corresponding fluorescence spectra in much detail. Therefore, also no information is obtained here on the formation of metastable

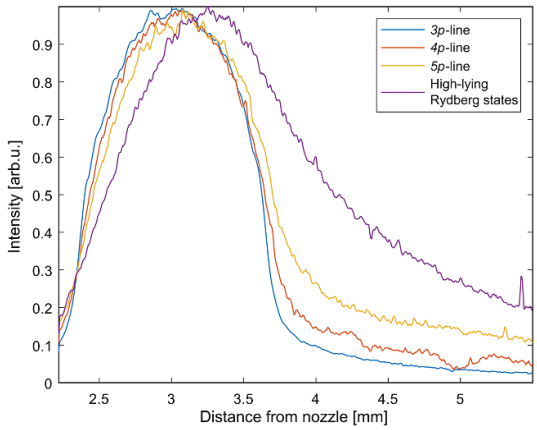

Figure 3. Normalized vertical readout of the cluster spectrum ($\overline{N} = 1.2 \times 10^6$). The profiles were obtained by integrating the intensity of camera pixels, which record fluorescence light within the wavelength range of 25.84 nm $< \lambda <$ 25.43 nm ($3p$), 24.46 nm $< \lambda <$ 24.16 nm ($4p$), 23.88 nm $< \lambda <$ 23.63 nm ($5p$) and 23.59 nm $< \lambda <$ 22.77 nm for the broadband emission from high-lying Rydberg states.

bubble states in He droplets [50, 64–66], which nevertheless appears to be rather unlikely in the presence of ions in the laser-generated nanoplasma due to the strong Coulomb attraction. We argue that the high density of quasifree electrons inside fully ionized clusters combined with the enhanced scattering cross-section of the embedded He_n^{2+} snowballs promotes TBR into high-lying Rydberg states of the cations. In the case of illuminated He gas, no such quasifree electrons and snowballs exist. Here, the lack of local electron density maxima in the vicinity of laser-generated free ions results in a much reduced recombination rate into Rydberg states, which explains the absence of the corresponding spectrally broad emission band in figure 2(a).

The vertical displacement of the emission source point from high-lying Rydberg states and the tail of low-energy fluorescence lines toward larger nozzle distances share a common origin. It is due to cluster disintegration driven by Coulomb and hydrodynamic forces. Their rapidly increasing net charge in the course of massive energy deposition and outer ionization accompanied by the continuously increasing temperature of quasifree electrons drives the cluster expansion. This results in individual ions gaining up to several keV of kinetic energy. In between the population of low-energy p-states by frustrated tunneling ionization [67–72] or direct multi-photon excitation [73–75] during the laser–plasma interaction and its radiative transition to the 1s-state an ion with keV kinetic energy moves a distance away from the IR laser focus. Accordingly, the length of the tail should scale with the lifetime of the electronically excited state, i.e. with the third power of the n quantum number of the populated p-state. Note that corresponding tails in fluorescence lines emitted from a beam of atomic He (figure 2(a)) are missing, because compared to the cluster ion emitters, which move at high speed, an illuminated beam of atomic He emits fluorescence essentially in rest.

Qualitatively, we find exactly this behavior in our experiments as shown in figure 3, where the normalized vertical profiles of all detected fluorescence bands from illuminated clusters are plotted. The higher-lying p-state emission spectra do indeed show longer tails than the lower-lying ones. According to the literature, their lifetime vary from 374 ps for the 3p-state to 3.2 ns for the 6p-state [40]. Thus, the electronically excited ions with keV kinetic energy from the disintegrating cluster have more time to move away from the nozzle before radiative decay takes place. We note in passing that the long tails of the lower-lying fluorescence lines, as well as the general shape of the high-lying broadband Rydberg emission are asymmetric with regards to the vertical axis, although the Coulomb explosion and hydrodynamic expansion that causes these dynamical processes is isotropic in nature. A possible and straight forward explanation is simply that closer toward the nozzle the ion and atom density markedly increases, which significantly enhances self-absorption. The effect might block the light emitted by ions that are pushed toward the nozzle by the Coulomb explosion resulting in the asymmetry we detect in figure 2.

Next, we investigate the population of high-lying Rydberg states depending on the number of atoms per cluster in the range of $10^4 < \overline{N} < 10^{10}$. With the cluster jet located at the laser beam waist, the temperature of the cryostat was varied to change the particle size across the different regimes of cluster formation: supersonic gas expansion, cluster formation close to the critical point, and the formation of the largest He droplets by liquid He fragmentation [76]. As shown in figure 4(a), the total fluorescence yield of the Rydberg emission increases by more than four orders of magnitude with cluster size across the measured size range and the same holds true for the 3p-fluorescence line. The dramatic signal increase is caused by the increased mass flow through the nozzle at low temperatures. Additionally, the opening angle of the He jet after leaving

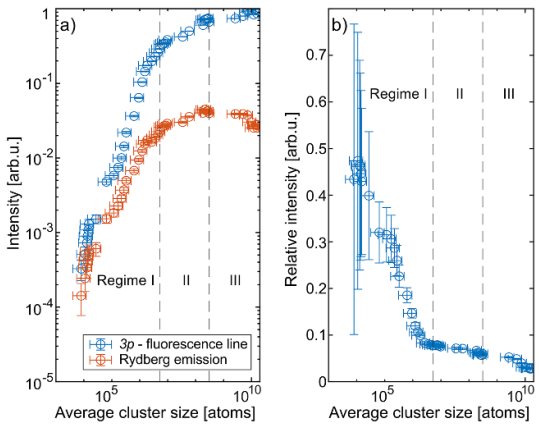

Figure 4. (a) Total yield of the 3*p*-fluorescence line and the Rydberg emission recorded as a function of average cluster size $\overline{N}$. (b) Relative intensity of the Rydberg emission compared to 3*p*-fluorescence depending on $\overline{N}$. Dashed vertical lines indicate different regimes of cluster formation: supersonic gas expansion (I), cluster formation close to the critical point (II), and the formation of the largest droplets by fragmentation out of the liquid phase (III).

the nozzle decreases with lower temperatures and therefore with larger average cluster sizes. Both effects lead to a higher He density in the focus volume resulting in a stronger fluorescence signal. For the largest average droplet size the total fluorescence yield does not increase further. The reason is that light propagation effects become important within clusters measuring several hundred nanometers to a few micrometers in diameter. These droplets are too large to be fully ionized by the laser pulse and the emission is partially self-absorbed in the outer shells. Furthermore, the emission from inner parts of the droplets is quenched by collision-induced non-radiative decay processes mediated by the quasifree electrons. These arguments are based on theoretical works modelling the interaction between laser light and nanoparticles on microscopic length scales [77]. The studies take into account: (i) classical trajectories of all electrons and ions fully resolving microscopic processes such as collisions and (ii) capture wave propagation phenomena, which take place on the order of the laser wavelength. The analysis of these processes has become possible through the recent development of the microscopic particle-in-cell (MicPIC) approach [78, 79]. The simulations show reduced MicPIC absorption for large clusters compared to electrostatic molecular dynamics simulations, which reflects radiation damping as a clear sign of propagation effects in the nanoplasma.

Interestingly, the relative signal strength of the Rydberg emission and the 3*p*-fluorescence depends on the cluster size N as displayed in figure 4(b). It shows a maximum for clusters comprising on average 10^4–10^5 atoms, i.e. close to the minimum size needed ($N = 10^5$) to support multiple charges in He clusters [46], a plateau in the size range 10^6–10^8 atoms and a decay for the largest droplets generated by fragmentation out of the liquid phase. Obviously, the relative population of high-lying Rydberg states exhibit a resonance behavior, which is similar to experimental observations and theoretical findings in previous nanoplasma studies on rare-gas clusters (see [80] and references therein). It results from the dynamic interplay of cluster ionization, quasifree electron heating and nanoplasma expansion. The individual time-dependent rates depend on cluster size and laser parameters. During the resonance phase the cluster absorbs laser radiation extremely efficiently and rapidly heats up, which in turn accelerates its expansion rate. After the laser pulse has passed the cluster and any heating dynamics have stopped, the expansion of the cluster still continues. This leads to a steady reduction in the temperature of the electrons due to adiabatic cooling. Once the electron temperature has dropped far enough that electron–ion recombination sets in according to the bottleneck model, strong fluorescence from high-lying Rydberg states is observed.

From the data we also learn that the population of high-lying Rydberg states in small He clusters comprising significantly less than 10^4 atoms appears to be a rather rare event, since the quasifree electrons and ions rapidly expand and leave the clusters within less than 1 ps. The capability of larger He droplets to trap ions and electrons in stable complexes and quasifree states, respectively, thereby accumulating multiple charge carriers over longer periods of time, promotes TBR in the laser-driven nanoplasma. Our findings complement recent studies on the XUV activation of He nanodroplets, where long-lasting changes of the strong-field optical properties of nanoparticles have been observed and attributed to electrons remaining loosely bound to photoions forming stable snowball structures in the droplets [41].

As the heating of the nanoplasma depends sensitively on the laser pulse duration also the relative population of high-lying Rydberg states for a given cluster size should show some resonant character is this respect. Indeed, this has been observed in the present study. The recorded fluorescence yields of the 3*p*-line

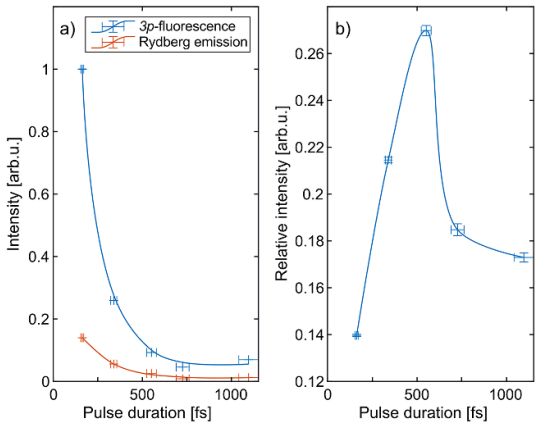

Figure 5. (a) Total yield of the 3*p*-fluorescence line and the Rydberg emission as a function of laser pulse length for clusters consisting $\overline{N} = 1.2 \times 10^6$ atoms and a pulse energy of 1 mJ. (b) Ratio of the intensity of the Rydberg emission to the 3*p*-fluorescence line. Solid lines are added as guide to the eye.

and the Rydberg emission are plotted in figure 5(a) as a function of the laser pulse duration. The experiments were carried out at a cluster size of $\overline{N} = 1.2 \times 10^6$ atoms varying the pulse duration between 180 fs and 1.2 ps. Depending on the setting of the grating compressor of the near-IR laser system the pulses contain different amounts of dispersion causing them to get stretched in time, which is characterized by recording intensity autocorrelation traces.

One can clearly see that both the strength of the 3*p*-fluorescence line and the Rydberg emission increases, when the clusters interact with pulses of the same energy but shorter duration. This is to be expected since shorter pulses with the same energy result in higher laser peak intensity and thus more efficient energy absorption. Note, the plasma heating rate increases with the ponderomotive potential and therefore also with the intensity of the drive laser. However, when plotting the relative strength of these emissions from electronically excited states populated in the transient nanoplasma as a function of laser pulse duration as done in figure 5(b) the resonance is revealed. The emission from high-lying Rydberg states mediated by TBR is strongest relative to the 3*p*-fluorescence in the nanoplasma at a pulse duration of 500 fs. Since in the present measurement the clusters are larger than those generating the strongest Rydberg ($>6p$) emission with a pulse duration of 180 fs (see figure 4(b)), one expects slightly longer pulses to reach the resonant condition for efficient laser energy absorption. This is because, larger droplets turned into a nanoplasma expand more slowly as the inner part remains quasi-neutral and electrons and ion remain confined in the plasma for longer periods of time [81]. We note in passing that we recorded the total fluorescence yield of the 3*p*-fluorescence line and the broadband Rydberg emission also as a function of laser pulse energy at a fixed pulse duration of 180 fs for clusters comprising $\overline{N} = 1.2 \times 10^6$ atoms. Under these conditions the population of the electronically excited states scales linearly with the deposited energy into the nanoplasma (not shown here).

Finally, we would like to briefly discuss the topic of coherence in the XUV nanoplasma emission induced by intense laser fields, which is of course a very interesting phenomena not only from an application point of view but also for basic research in attosecond physics. High-harmonic generation (HHG) in small nanoparticles of the heavier rare gases has been demonstrated in the past [82–86]. However, in the present study on large helium droplets exposed to strong laser fields we did not observe HHG, neither above the ionization threshold nor below, i.e. spectrally overlapping with the atomic Rydberg resonance energies. The likely reason is the use of rather long laser pulses with a duration of 180 fs, which corresponds to 52 optical cycles at a wavelength of 1030 nm. With such a large number of cycles it is likely that the cluster has been transformed into a helium nanoplasma before the peak intensity is reached, where efficient generation of XUV light typically occurs. It seems that once the transient nanoplasma is created the phase relation between the drive laser field and the generated XUV light in the dense heterogeneous medium is lost, which prevents the so-called phase matching condition in HHG to be fulfilled [87].

In the case of the strong-field interaction with a beam of atomic He (figure 2(a)), given the wavelength $\lambda = 1030$ nm and the focal spot size of 6 μm, we obtain a minimum phase matching pressure 4.5 mbar. Considering that the gas nozzle has a diameter of 5 μm and we apply a pressure of 20 bar and assuming an opening angle of 45° for the gas jet, we obtain the 4.5 mbar at a distance from the nozzle of 166 μm. This is much closer to the nozzle than the 3 mm used in the experiment. Therefore, we could also not achieve phase matching and observe coherent HHG emission in the beam of atomic He (figure 2(a)). Nevertheless, we would like to emphasize that the population of Rydberg states in atoms by intense fs laser pulses is a coherent

process and all atoms in the gas medium decay in phase to the ground state by spontaneous emission, resulting in coherent emission typically referred to as XUV free induction decay (XFID) [73].

In atoms it has been shown that the coherent emission of Rydberg states in the extreme ultraviolet spectral range can also be populated by recapture of the tunneling electrons during the interaction with the laser field in addition to resonant multi-photon excitation [72]. This is very similar to HHG, because recombination to the excited state occurs after excursion along electron trajectories generating XFID pulses of nanosecond duration. It would be extremely interesting to study the temporal properties of the XUV nanoplasma emission by using for instance the so-called attosecond lighthouse technique [88, 89]. The attosecond lighthouse maps the emission time onto the propagation direction and therefore provides important information on the temporal confinement of the emission from Rydberg states. However, the application of this advanced technology developed by the attosecond science community using atomic targets goes beyond the scope of the present nanoplasma study.

In summary, utilizing fluorescence spectroscopy to investigate energy absorption and dissipation in helium clusters and large droplets irradiated with intense fs laser pulses at central wavelength of 1030 nm revealed a number of interesting phenomena. First of all, it is clearly observed, how the dense cluster environment opens up an additional relaxation pathway in the laser-generated nanoplasma via TBR in comparison to the laser interaction with a beam of He atoms. The nanoplasma-specific relaxation pathway results in the population of high-lying Rydberg states of He ions upon plasma expansion and adiabatic electron cooling, respectively. The fluorescence decay into the ionic ground state results in a characteristic broadband emission of XUV photons with energies close to the ionization potential of He^+. This finding is in agreement with previous studies using electron and ion spectroscopy to unravel the role of Rydberg states in the energetics and dynamics of laser-generated nanoplasma. The XUV spectrometer setup in the present work, which also acts as a pinhole camera, allowed to make qualitative statements about the relative time frame of the TBR relaxation pathway by a time to space mapping of the fluorescence source point in the expanding nanoplasma. This is because the cluster has to expand, i.e. the electrons need to thermalize before high-lying Rydberg-states are efficiently populated by low-energy quasifree plasma electrons according to the well-known bottleneck model. By varying the size of the clusters, we were able to study the size-dependence of the resonant plasma heating, since the TBR relaxation pathway is much more sensitive to the temperature of quasifree electrons than is fluorescence from direct laser excitation of low-lying electronic states also populated in the plasma. Last but not least, we were able to corroborate the electron-temperature sensitivity of TBR by influencing the resonant heating condition applying laser pulses of different duration.

Data availability statement

All data that support the findings of this study are included within the article (and any supplementary files).

Acknowledgment

This research was supported by the German Federal Ministry for Economic Affairs and Climate Action through the collaborative ZIM research Project KK5322301DF1.

ORCID iD

Tim Laarmann https://orcid.org/0000-0003-4289-8536

References

[1] Krainov V and Smirnov M 2002 Cluster beams in the super-intense femtosecond laser pulse *Phys. Rep.* **370** 237
[2] Saalmann U, Siedschlag C and Rost J M 2006 Mechanisms of cluster ionization in strong laser pulses *J. Phys. B: At. Mol. Opt. Phys.* **39** R39
[3] Fennel T, Meiwes-Broer K-H, Tiggesbäumker J, Reinhard P-G, Dinh P M and Suraud E 2010 Laser-driven nonlinear cluster dynamics *Rev. Mod. Phys.* **82** 1793
[4] Krishnan S R, Gopal R, Rajeev R, Jha J, Sharma V, Mudrich M, Moshammer R and Krishnamurthy M 2014 Photoionization of clusters in intense few-cycle near infrared femtosecond pulses *Phys. Chem. Chem. Phys.* **16** 8721
[5] Schütte B, Ye P, Patchkovskii S, Austin D R, Brahms C, Strüber C, Witting T, Ivanov M Y, Tisch J W G and Marangos J P 2016 Strong-field ionization of clusters using two-cycle pulses at 1.8 μm *Sci. Rep.* **6** 39664
[6] Wabnitz H *et al* 2002 Multiple ionization of atom clusters by intense soft x-rays from a free-electron laser *Nature* **420** 482
[7] Schulz J, Wabnitz H, Laarmann T, Gürtler P, Laasch W, Swiderski A, Möller T and de Castro A 2003 Energy absorption of free rare gas clusters irradiated by intense VUV pulses of a free electron laser *Nucl. Instrum. Methods Phys. Res.* A **507** 572
[8] Laarmann T, de Castro A R B, Gürtler P, Laasch W, Schulz J, Wabnitz H and Möller T 2004 Interaction of argon clusters with intense VUV-laser radiation: the role of electronic structure in the energy-deposition process *Phys. Rev. Lett.* **92** 143401

[9] Laarmann T, Rusek M, Wabnitz H, Schulz J, de Castro A R B, Gürtler P, Laasch W and Möller T 2005 Emission of thermally activated electrons from rare gas clusters irradiated with intense VUV light pulses from a free-electron laser *Phys. Rev. Lett.* **95** 063402
[10] Ziaja B, Laarmann T, Wabnitz H, Wang F, Weckert E, Bostedt C and Möller T 2009 Emission of electrons from rare gas clusters after irradiation with intense VUV pulses of wavelength 100 nm and 32 nm *New J. Phys.* **11** 103012
[11] Pandit R, Bigaouette N, Becker V R, Thurston J, Barrington K, Ackad E and Ramunno L 2019 Intense VUV–xenon-cluster interaction revisited *Phys. Rev.* A **100** 063402
[12] Hoener M, Bostedt C, Thomas H, Landt L, Eremina E, Wabnitz H, Laarmann T, Treusch R, de Castro A R B and Möller T 2008 Charge recombination in soft x-ray laser produced nanoplasmas *J. Phys.* B **41** 181001
[13] Bostedt C *et al* 2012 Ultrafast x-ray scattering of xenon nanoparticles: imaging transient states of matter *Phys. Rev. Lett.* **108** 093401
[14] Thomas H *et al* 2012 Explosions of xenon clusters in ultraintense femtosecond x-ray pulses from the LCLS free-electron laser *Phys. Rev. Lett.* **108** 133401
[15] Gorkhover T *et al* 2012 Nanoplasma dynamics of single large xenon clusters irradiated with superintense x-ray pulses from the linac coherent light source free-electron laser *Phys. Rev. Lett.* **108** 245005
[16] Springate E, Aseyev S A, Zamith S and Vrakking M J J 2003 Electron kinetic energy measurements from laser irradiation of clusters *Phys. Rev.* A **68** 053201
[17] Snyder E M, Buzza S A Jr and Castleman A W 1996 Intense field-matter interactions: multiple ionization of clusters *Phys. Rev. Lett.* **77** 3347
[18] Lezius M, Dobosz S, Normand D and Schmidt M 1998 Explosion dynamics of rare gas clusters in strong laser fields *Phys. Rev. Lett.* **80** 261
[19] McPherson A, Thompson B D, Borisov A B, Boyer K and Rhodes C K 1994 Multiphoton-induced x-ray emission at 4–5 keV from Xe atoms with multiple core vacancies *Nature* **370** 631
[20] Ditmire T, Zweiback J, Yanovsky V P, Cowan T E, Hays G and Wharton K B 1999 Nuclear fusion from explosions of femtosecond laser-heated deuterium clusters *Nature* **398** 489
[21] Schütte B *et al* 2018 Low-energy electron emission in the strong-field ionization of rare gas clusters *Phys. Rev. Lett.* **121** 063202
[22] Schütte B, Arbeiter M, Fennel T, Jabbari G, Kuleff A I, Vrakking M J J and Rouzée A 2015 Observation of correlated electronic decay in expanding clusters triggered by near-infrared fields *Nat. Commun.* **6** 8596
[23] Oelze T *et al* 2017 Correlated electronic decay in expanding clusters triggered by intense XUV pulses from a free-electron-laser *Sci. Rep.* **7** 40736
[24] Niozu A *et al* 2019 Electron spectroscopic study of nanoplasma formation triggered by intense soft x-ray pulses *J. Chem. Phys.* **151** 184305
[25] Schütte B, Campi F, Arbeiter M, Fennel T, Vrakking M J J and Rouzée A 2014 Tracing electron-ion recombination in nanoplasmas produced by extreme-ultraviolet irradiation of rare-gas clusters *Phys. Rev. Lett.* **112** 253401
[26] Ackad E, Bigaouette N, Mack S, Popov K and Ramunno L 2013 Recombination effects in soft-x-ray cluster interactions at the xenon giant resonance *New J. Phys.* **15** 053047
[27] Schütte B, Oelze T, Krikunova M, Arbeiter M, Fennel T, Vrakking M J J and Rouzée A 2015 Recombination dynamics of clusters in intense extreme-ultraviolet and near-infrared fields *New J. Phys.* **17** 033043
[28] Schroedter L *et al* 2014 Hidden charge states in soft-x-ray laser-produced nanoplasmas revealed by fluorescence spectroscopy *Phys. Rev. Lett.* **112** 183401
[29] Müller M *et al* 2015 Ionization dynamics of XUV excited clusters: the role of inelastic electron collisions *J. Phys. B: At. Mol. Opt. Phys.* **48** 174002
[30] Przystawik A *et al* 2015 Ionization dynamics of Xe nanoplasma formation studied with XUV fluorescence spectroscopy *J. Phys. B: At. Mol. Opt. Phys.* **48** 184002
[31] Kelbg M, Zabel M, Krebs B, Kazak L, Meiwes-Broer K-H and Tiggesbäumker J 2019 Auger emission from the Coulomb explosion of helium nanoplasmas *J. Chem. Phys.* **150** 204302
[32] Kelbg M, Zabel M, Krebs B, Kazak L, Meiwes-Broer K-H and Tiggesbäumker J 2020 Temporal development of a laser-induced helium nanoplasma measured through Auger emission and above-threshold ionization *Phys. Rev. Lett.* **125** 093202
[33] Hahn Y 1997 Electron-ion recombination processes - an overview *Rep. Prog. Phys.* **60** 691
[34] Mansbach P and Keck J 1969 Monte Carlo trajectory calculations of atomic excitation and ionization by thermal electrons *Phys. Rev.* **181** 275
[35] Hu S X 2007 Three-body recombination of atomic ions with slow electrons *Phys. Rev. Lett.* **98** 133201
[36] Gomez L F, Loginov E, Sliter R and Vilesov A F 2011 Sizes of large He droplets *J. Chem. Phys.* **135** 154201
[37] Augst S, Strickland D, Meyerhofer D D, Chin S L and Eberly J H 1989 Tunneling ionization of noble gases in a high-intensity laser field *Phys. Rev. Lett.* **63** 2212
[38] Döppner T, Müller J P, Przystawik A, Göde S, Tiggesbäumker J, Meiwes-Broer K-H, Varin C, Ramunno L, Brabec T and Fennel T 2010 Steplike intensity threshold behavior of extreme ionization in laser-driven xenon clusters *Phys. Rev. Lett.* **105** 053401
[39] Hanafi M, Omar M and Gamal Y-D 2000 Study of laser-induced breakdown spectroscopy of gases *Radiat. Phys. Chem.* **57** 11
[40] Wiese W L and Fuhr J R 2009 Accurate atomic transition probabilities for hydrogen, helium and lithium *J. Phys. Chem. Ref. Data* **38** 565
[41] Medina C *et al* 2023 Long-lasting XUV activation of helium nanodroplets for avalanche ionization *New. J. Phys.* **25** 053030
[42] Heidenreich A, Schomas D and Mudrich M 2017 Dopant-induced ignition of helium nanoplasmas-a mechanistic study *J. Phys. B: At. Mol. Opt. Phys.* **50** 244001
[43] Atkins K 1959 Ions in liquid helium *Phys. Rev.* **116** 1339
[44] Johnson W W and Glaberson W I 1972 Positive impurity ions in He II *Phys. Rev. Lett.* **29** 214
[45] González-Lezana T, Echt O, Gatchell M, Bartolomei M, Campos-Martínez J and Scheier P 2020 Solvation of ions in helium *Int. Rev. Phys. Chem.* **39** 465
[46] Laimer F, Kranabetter L, Tiefenthaler L, Albertini S, Zappa F, Ellis A M, Gatchell M and Scheier P 2019 Highly charged droplets of superfluid helium *Phys. Rev. Lett.* **123** 165301
[47] Feinberg A J *et al* 2022 X-ray diffractive imaging of highly ionized helium nanodroplets *Phys. Rev. Res.* **4** L022063
[48] Rosenblit M and Jortner J 1995 Dynamics of the formation of an electron bubble in liquid helium *Phys. Rev. Lett.* **75** 4079
[49] Fárník M, Henne U, Samelin B and Toennies J P 1997 Comparison between positive and negative charging of helium droplets *Z. Phys.* D **40** 93

[50] Fárník M, Henne U, Samelin B and Toennies J P 1998 Differences in the detachment of electron bubbles from superfluid ^{4}He droplets versus nonsuperfluid ^{3}He droplets *Phys. Rev. Lett.* **81** 3892
[51] Buchenau H, Toennies J and Northby J 1991 Excitation and ionization of ^{4}He clusters by electrons *J. Chem. Phys.* **95** 8134
[52] von Haeften K, Laarmann T, Wabnitz H and Möller T 2001 Observation of atomiclike electronic excitations in pure ^{3}He and ^{4}He clusters studied by fluorescence excitation spectroscopy *Phys. Rev. Lett.* **87** 153403
[53] von Haeften K, Laarmann T, Wabnitz H, Möller T and Fink K 2011 Size and isotope effects of helium clusters and droplets: identification of surface and bulk-volume excitations *J. Phys. Chem.* A **115** 7316
[54] Mauracher A, Echt O, Ellis A, Yang S, Bohme D, Postler J, Kaiser A, Denifl S and Scheier P 2018 Cold physics and chemistry: collisions, ionization and reactions inside helium nanodroplets close to zero K *Phys. Rep.* **751** 1–90
[55] von Haeften K, Laarmann T, Wabnitz H and Möller T 2005 The electronically excited states of helium clusters: an unusual example for the presence of Rydberg states in condensed matter *J. Phys. B: At. Mol. Opt. Phys.* **38** S373
[56] Loginov E and Drabbels M 2011 Unusual Rydberg system consisting of a positively charged helium nanodroplet with an orbiting electron *Phys. Rev. Lett.* **106** 083401
[57] Peterka D S, Lindinger A, Poisson L, Ahmed M and Neumark D M 2003 Photoelectron imaging of helium droplets *Phys. Rev. Lett.* **91** 043401
[58] Asmussen J D *et al* 2021 Unravelling the full relaxation dynamics of superexcited helium nanodroplets *Phys. Chem. Chem. Phys.* **23** 15138
[59] Ovcharenko Y *et al* 2020 Autoionization dynamics of helium nanodroplets resonantly excited by intense XUV laser pulses *New J. Phys.* **22** 083043
[60] LaForge A C *et al* 2021 Ultrafast resonant interatomic Coulombic decay induced by quantum fluid dynamics *Phys. Rev.* X **11** 021011
[61] Kornilov O, Bünermann O, Haxton D J, Leone S R, Neumark D M and Gessner O 2011 Femtosecond photoelectron imaging of transient electronic states and Rydberg atom emission from electronically excited He droplets *J. Phys. Chem.* A **115** 7891
[62] Mudrich M *et al* 2020 Ultrafast relaxation of photoexcited superfluid He nanodroplets *Nat. Commun.* **11** 112
[63] von Haeften K, Laarmann T, Wabnitz H and Möller T 2023 Relaxation dynamics of ^{3}He and ^{4}He clusters and droplets studied using near infrared and visible fluorescence excitation spectroscopy *Phys. Chem. Chem. Phys.* **25** 1863–80
[64] Jiang T, Kim C and Northby J A 1993 Electron attachment to helium microdroplets: creation induced magic? *Phys. Rev. Lett.* **71** 700
[65] Henne U and Toennies J P 1998 Electron capture by large helium droplets *J. Chem. Phys.* **108** 9327
[66] von Haeften K, Laarmann T, Wabnitz H and Möller T 2002 Bubble formation and decay in ^{3}He and ^{4}He clusters *Phys. Rev. Lett.* **88** 233401
[67] Nubbemeyer T, Gorling K, Saenz A, Eichmann U and Sandner W 2008 Strong-field tunneling without ionization *Phys. Rev. Lett.* **101** 233001
[68] Landsman A S, Pfeiffer A N, Hofmann C, Smolarski M, Cirelli C and Keller U 2013 Rydberg state creation by tunnel ionization *New J. Phys.* **15** 013001
[69] Eichmann U, Saenz A, Eilzer S, Nubbemeyer T and Sandner W 2013 Observing rydberg atoms to survive intense laser fields *Phys. Rev. Lett.* **110** 203002
[70] Xiong W-H, Xiao X-R, Peng L-Y and Gong Q 2016 Correspondence of below-threshold high-order-harmonic generation and frustrated tunneling ionization *Phys. Rev.* A **94** 013417
[71] Zimmermann H, Patchkovskii S, Ivanov M and Eichmann U 2017 Unified time and frequency picture of ultrafast atomic excitation in strong laser fields *Phys. Rev. Lett.* **118** 013003
[72] Yun H, Mun J H, Hwang S I, Park S B, Ivanov I A, Nam C H and Kim K T 2018 Coherent extreme-ultraviolet emission generated through frustrated tunnelling ionization *Nat. Photon.* **12** 620
[73] Beaulieu S *et al* 2016 Role of excited states in high-order harmonic generation *Phys. Rev. Lett.* **117** 203001
[74] Bengtsson S *et al* 2017 Space-time control of free induction decay in the extreme ultraviolet *Nat. Photon.* **11** 252
[75] Beaulieu S, Bloch E, Barreau L, Comby A, Descamps D, Géneaux R, Légaré F, Petit S and Mairesse Y 2017 Phase-resolved two-dimensional spectroscopy of electronic wave packets by laser-induced XUV free induction decay *Phys. Rev.* A **95** 041401
[76] Toennies J P and Vilesov A F 2004 Superfluid helium droplets: a uniquely cold nanomatrix for molecules and molecular complexes *Angew. Chem., Int. Ed.* **43** 2622
[77] Varin C, Peltz C, Brabec T and Fennel T 2014 Light wave driven electron dynamics in clusters *Ann. Phys., Lpz.* **526** 135
[78] Peltz C, Varin C, Brabec T and Fennel T 2012 Fully microscopic analysis of laser-driven finite plasmas using the example of clusters *New J. Phys.* **14** 065011
[79] Varin C, Peltz C, Brabec T and Fennel T 2012 Attosecond plasma wave dynamics in laser-driven cluster nanoplasmas *Phys. Rev. Lett.* **108** 175007
[80] Saalmann U 2006 Resonant energy absorption of rare-gas clusters in strong laser pulses *J. Mod. Opt.* **53** 173
[81] Krishnan S R *et al* 2012 Evolution of dopant-induced helium nanoplasmas *New J. Phys.* **14** 075016
[82] Ruf H *et al* 2013 Inhomogeneous high harmonic generation in krypton clusters *Phys. Rev. Lett.* **110** 083902
[83] Tisch J W G, Ditmire T, Fraser D J, Hay N, Mason M B, Springate E, Marangos J P and Hutchinson M H R 1997 Investigation of high-harmonic generation from xenon atom clusters *J. Phys. B: At. Mol. Opt. Phys.* **30** L709
[84] Aladi M, Bolla R, Rácz P and Földes I 2016 Noble gas clusters and nanoplasmas in high harmonic generation *Nucl. Instrum. Methods Phys. Res.* B **369** 68
[85] Vozzi C *et al* 2005 Cluster effects in high-order harmonics generated by ultrashort light pulses *Appl. Phys. Lett.* **86** 111121
[86] Bódi B, Aladi M, Rácz P, Földes I B and Dombi P 2019 High harmonic generation on noble gas clusters *Opt. Express* **27** 26721
[87] Rundquist A, Durfee III C G, Chang Z, Herne C, Backus S, Murnane M M and Kapteyn H C 1998 Phase-matched generation of coherent soft x-rays *Science* **280** 1412
[88] Vincenti H and Quéré F 2012 Attosecond lighthouses: how to use spatiotemporally coupled light fields to generate isolated attosecond pulses *Phys. Rev. Lett.* **108** 113904
[89] Kim K T, Zhang C, Ruchon T, Hergott J-F, Auguste T, Villeneuve D M, Corkum P B and Quéré F 2013 Photonic streaking of attosecond pulse trains *Nat. Photon.* **7** 651